Journal of Fundamental and Applied Sciences

ISSN 1112-9867

Available online at http://www.jfas.info

SEARCH FOR STRUCTURAL SCAFFOLDS AGAINST SARS-COV-2 M^{PRO}: AN *IN SILICO* STUDY

E. Onah[1*], I. C. Ugwoke[1], U. J. Eze[1], H.C. Eze[1], S. K. Musa[2], S. Ndiana-Abasi[3], O. Okoli[4], I. E. Ekeh[5], A. A. Edet[6]

[1]Faculty of Pharmaceutical Sciences, University of Nigeria, Nsukka, Nigeria

[2]Faculty of Pharmacy, Ahmadu Bello University, Zaria, Kaduna State, Nigeria

[3]Faculty of Pharmacy, University of Uyo, Uyo, Nigeria

[4]Faculty of Pharmacy, University of Lagos, Lagos, Nigeria

[5]Faculty of Pharmacy, Rajiv Ghandi University of Health Science, Karnataka, India

[6]Faculty of Pharmaceutical Sciences, University of Port Harcourt, Rivers State, Nigeria

Received: 15 September 2020 / Accepted: 10 January 2021 / Published online: 01 May 2021

ABSTRACT

The emergence of the deadly SARS-CoV-2, the etiologic agent of COVID-19 towards the end of the fourth quarter of 2019 has necessitated intensive research towards the development of drugs and vaccine that can combat the disease. Consequently, we conducted molecular docking of the e-Drug3D library using London dG and Affinity dG as scoring algorithms for common structural scaffolds in drug molecules with strong binding affinities towards SARS-CoV-2 M^{pro}. 15 drug molecules forming about 0.8% of the library bound strongly to the target protein, which gave rise to Two potential structural scaffolds: (4S,4aR,5aR,12aS)-4-(dimethylamino)-10,12,12a-trihydroxy-1,11-dioxo-1,4,4a,5,5a,6,11,12a-octahydro-2-tetracenecarboxamide and the stilbenoid-like structure. These scaffolds could serve as potential starting points in the structure-based design of anti-SARS-CoV-2 drugs.

Keywords: SARS-CoV-2, COVID-19, M^{pro}, *in silico* techniques, structural scaffolds, ligand-protein interaction.

Author Correspondence, e-mail: emmanuel.onah.187260@unn.edu.ng

doi: http://dx.doi.org/10.43 14/jfas.v13i2.7

1. INTRODUCTION

Towards the end of the fourth quarter of 2019, a severe pneumonia-like viral disease with high mortality rate originating from the state of Wuhan in China spread to a pandemic level, causing severe havoc to humanity – economic, social and health wise [1]. In fact, as at September 9, 2020, the disease has affected 216 countries with a total of 27,205,275 cases have been reported globally with 890,392 deaths [2]. This disease has had a very massive impact on all facets of life. The virus responsible for this disease has been discovered to be of the same origin as the Coronavirus (CoV) responsible for the Severe Acute Respiratory Syndrome (SARS) disease called SARS-CoV [3]. Because the novel Coronavirus disease started in late 2019, it was named COVID-19 by the World Health Organization on the 11th of February, 2020 to reflect the year the disease started. Analogically, the etiologic agent responsible was named SARS-CoV-2 by the International Committee on Taxonomy of Viruses [3, 4]. Owing to the importance of COVID-19, scientists from all around the world have been working round the clock to find cure for the disease, but till date no definitive cure has been found [5]. However, a number of drug molecules both of natural and synthetic origin, most from list of FDA approved drugs have been shown to have inhibitory activity against SARS-CoV-2 [5, 6]. Some drugs reported to be used in the treatment of patients with COVID-19 include α-interferon, the antiretroviral drugs Lopinavir/Ritonavir and the broad spectrum antiviral drug Remdesivir, the antimalarial/antirheumatoid drugs Chloroquine and Hydroxychloroquine, Tocilizumab [4,7,8], among others. Nonetheless, more data are needed to prove the efficacy of these drugs. Effort is been made to produce a vaccine for the disease [9], but as the search continues the search drug molecules that can inhibit/treat the viral disease also need to continue.

Genomic sequencing has shown that this pathogenic coronavirus is identical and shares over 70% Gene sequence with SARS-CoV [9]. The SARS-CoV-2 main protease (M^{pro}) also called 3C-like protease ($3CL^{pro}$) is a conserved enzyme that plays a vital role in the life cycle of Coronaviruses (CoVs). M^{pro} contains three cysteine protease domains, I to III and is involved, alongside one or two papain-like proteases (PLPs), in most maturation cleavage events within the precursor polyproteins known as ppla and pp1ab. These polyproteins are cleaved into 16 nonstructural proteins (nsps) that engage in the production of subgenomic RNAs that encode four structural proteins called envelop (E), membrane (M), spike (S) and nucleocapsid (N) proteins [9-11]. The M^{pro} active sites are highly conserved among all CoVs M^{pro}s and several common characteristics

are shared among the substrates of M^{pro} in different CoVs [11]. Since M^{pro} is highly conserved among the CoVs and is important in the viral replication, and there is no human analog, it is considered an ideal antiviral drug target [12,13].

Molecular docking and virtual screening are some of the most used *in silico* approaches towards the discovery of molecules that could inhibit SARS-CoV-2. This is true because a viral disease with high magnitude of virulence requires rapid drug development approaches of which computer-aided drug design readily offers promising solutions [10]. Gimeno [10] applied virtual screening to rapidly identify commercial drugs that could be repurposed for COVID-19 treatment. In a study carried out by Fischer [14] 606 million compounds were screen using virtual screening for potential inhibitors for the novel Coronavirus protease. Similarly, Ton [15] carried out deep-docking of over 1 billion compounds for the identification of potential inhibitors of SARS-CoV-2 main protease. These computational approaches to drug discovery are particularly important because they accelerate and economize drug discovery process [16]. However, *in silico* approaches of drug development do not serve as a complete replacement for traditional methods of drug discovery as both should work in unison towards a faster and attrition free drug discovery.

In this study, we used computational techniques to screen about 2000 FDA approved drug molecules retrieved from e-Drug3D library [17], an online database in search for potential structural scaffolds of drug molecules that can bind to SARS-CoV 2 M^{pro}.

2. RESULTS AND DISCUSSION

Recent studies have characterized the pharmacophoric features and types of ligand-protein interactions a drug molecule must exhibit with the key amino acid residues resident at the active site of SARS-CoV-2 M^{pro} for potent inhibitory effect [9,12,21-24]. His41 and Cys145 residues are responsible for the catalytic activity of M^{pro} and because of this, they are often referred to as "M^{pro} catalytic dyad His41-Cys145" [5, 9, 10, 23]. Glu166 plays a role in the dimerization of M^{pro} by interacting with each of the N-finger of the two promoters that shapes the S1 pocket for substrate-binding, a process which is also necessary for the catalytic activity of the enzyme [21]. Yoshino [22] conducted an *in silico* study that showed that besides His41, Cys145 and Glu166, other amino acid residues like Ser144, Gly143 and Gln189 also interact with pharmacophoric moieties present on inhibitors hence, ligand-protein interaction with these amino acid residues also promote binding of inhibitors to SARS-CoV-2 M^{pro}. Other amino acid residues necessary for binding and stabilizing

of the ligand-protein complex via H-bonds and π-hydrogen bonds include but not limited to Thr190, His164, Asn142, Leu168, Phe140, Met49 and Leu27 [23]. Very importantly, structural analysis has shown that M^{pro} binding site has very restricted flexibility with the S1 pocket being particularly rigid, changing only slightly at the end of the Ser1 and Asn142 residues of the side chains [10]. Owing to this, we assumed the receptor binding pocket to be rigid for all the molecular docking studies performed.

Re-docking of the cocrystallized ligand 11b **(**N-[(2S)-3-(3-fluorophenyl)-1-oxidanylidene-1-[[(2S)-1-oxidanylidene-3-[(3S)-2-oxidanylidenepyrrolidin-3-yl]propan-2-yl]amino]propan-2-yl]-1H-indole-2-carboxamide**)** to the active site of the protease using the same docking protocol resulted in the binding of the ligand in the same position and orientation as the cocrystallized inhibitor. Figure 1A and 1B show the docked pose of 11b superimposed on the cocrystallized structure and the binding pocket of 11b on SARS-CoV-2 M^{pro} active site respectively. This proves that the docking parameters chosen are optimal. The docking parameters for the grid box obtained during the validation phase are shown in table 1.

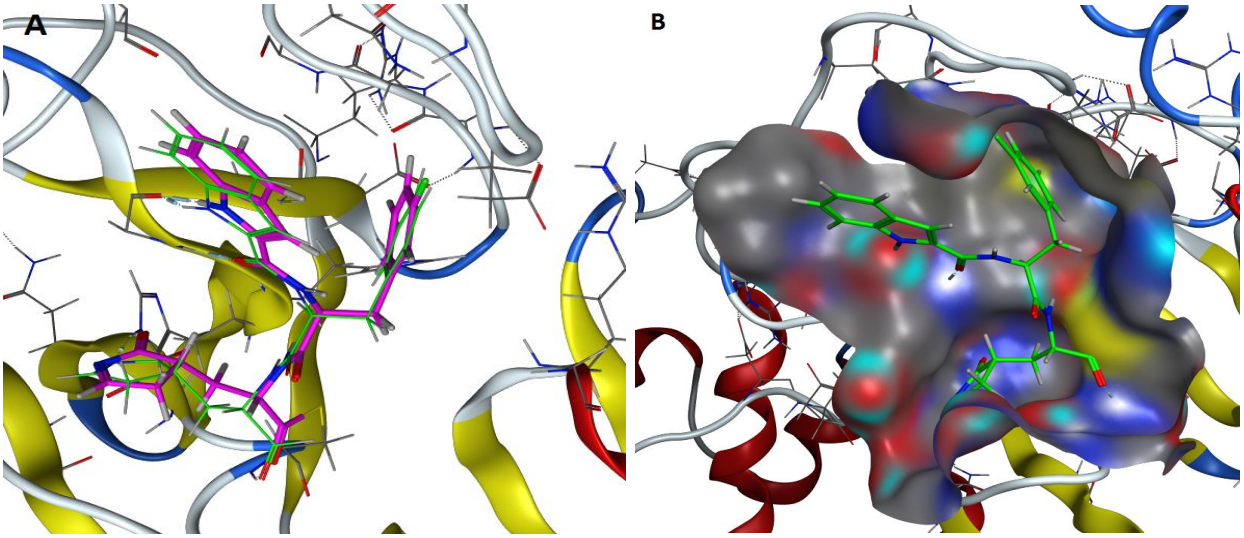

Fig.1. (A) The docked pose of 11b (green) superimposed on the cocrystallized structure (purple). (B) Binding pocket of 11b on SARS-CoV-2 M^{pro} active site

Table 1: Docking validation parameters and results

Grid Box Origin			Grid Box Radius			RMSD	London dG score (Kcal/mol)	Affinity dG score (Kcal/mol)
X	Y	Z	X	Y	Z			
-12.2425	11.6588	68.5006	8.0	8.0	8.0	1.5565	-11.4869	-4.9094

The best pose of the re-docked cocrystallized inhibitor 11b **(**N-[(2S)-3-(3-fluorophenyl)-1-oxidanylidene-1-[[(2S)-1-oxidanylidene-3-[(3S)-2-oxidanylidenepyrrolidin-3-yl]propan-2-yl]amino]propan-2-yl]-1H-indole-2-carboxamide) with the least RMSD and most negative affinity binding scores for both London dG and affinity dG (Table 1) exhibited several ligand-protein interactions of interest. 11b belongs to the class of α-ketoamides, a class of compounds that have been shown in several studies to have potent inhibitory effect on SARS-CoV-2 M^{pro} [5,9,12]. The following ligand protein interactions shown in figure 2 were observed for the re-docked native ligand. Glu166 donated 3.21-Å H-bond to the Oxygen atom of the α-ketoamido group linking the 1H-indole moiety to the rest of the molecule. Glu166 also accepted 2.95-Å H-bond from the nitrogen atom of the 1H-indole moiety. His163 donated 3.67-Å H-bond to the nitrogen atom of 2-oxidanylidenepyrrolidine moiety. Finally, Gly143 donated 3.1-Å H-bond to the oxygen atom of the 1-oxidanylidene moiety. These findings further support the docking protocol validation as it reproduced a number of the ligand-protein interactions observed in the cocrystallized inhibitor (Figure 2). However, other ligand-protein interactions found on the cocrystallized inhibitor not modeled in our re-docked structure include: 3.83-Å π-hydrogen bond interaction between the His41 and the 3-flourobenzyl moiety via the C1 hydrogen atom of the propane backbone. His164 donated 2.94-Å H-bond to the Nitrogen atom of α-ketoamido group linking the 1H-indole moiety to the rest of the molecule. The oxygen atom of the 1-oxidanylidene moiety accepted 2.5-Å H-bond from the His163 residue. Nonetheless, these interactions were still considered in the discussion of our best scoring drugs.

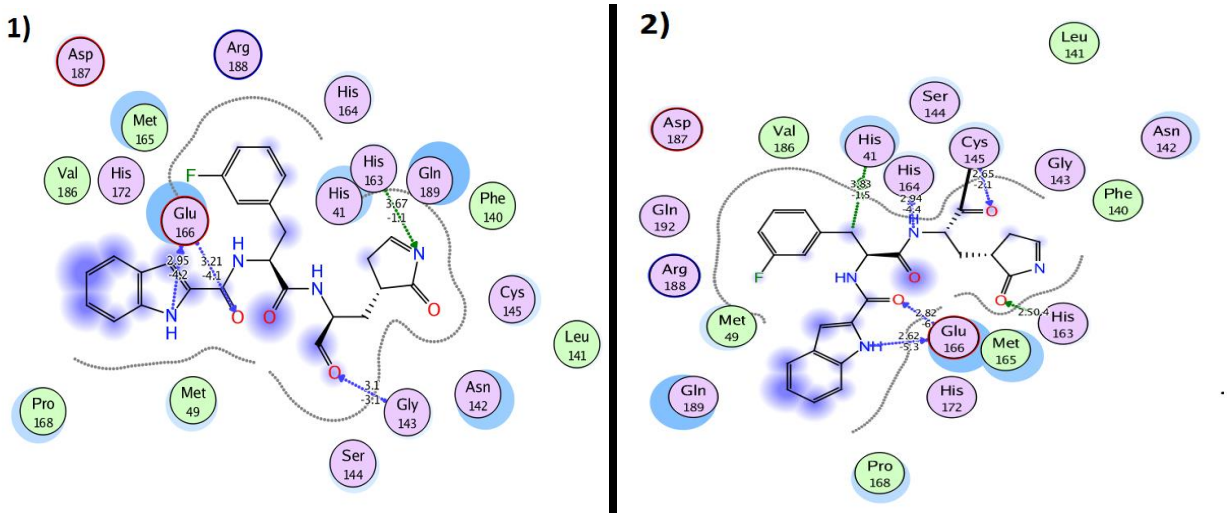

Fig.2. Comparison of the ligand-protein interactions of the best poses of: 1) the re-docked inhibitor and 2) the cocrystallized inhibitor

The results of the molecular docking showed that the docking energies from the two scoring functions London dG and Affinity dG followed the normal or Gaussian distribution ranging from < -14.0 Kcal/mol to > -2.0 Kcal/mol for London dG and < -8.0 Kcal/mol to > 0.0 Kcal/mol for Affinity dG (see figure 3). The London dG scoring function estimates the free energy of binding of the ligand from a given pose, as a combination of several terms, including the average rotational and translational entropy terms, energy lost as a result of the flexibility of the ligand, hydrogen bonding, metal contacts, and a desolvation term due to the volumes of the atoms of the protein and ligand in contact with the solvent [25]. The Affinity dG scoring estimates the enthalpic contribution to the free energy of binding and takes into consideration the atomic contributions to the enthalpic term, including H-bond donor/acceptor pairs, Coulomb interactions between ions, metal ligation, hydrophobic contributions, etc. [25].

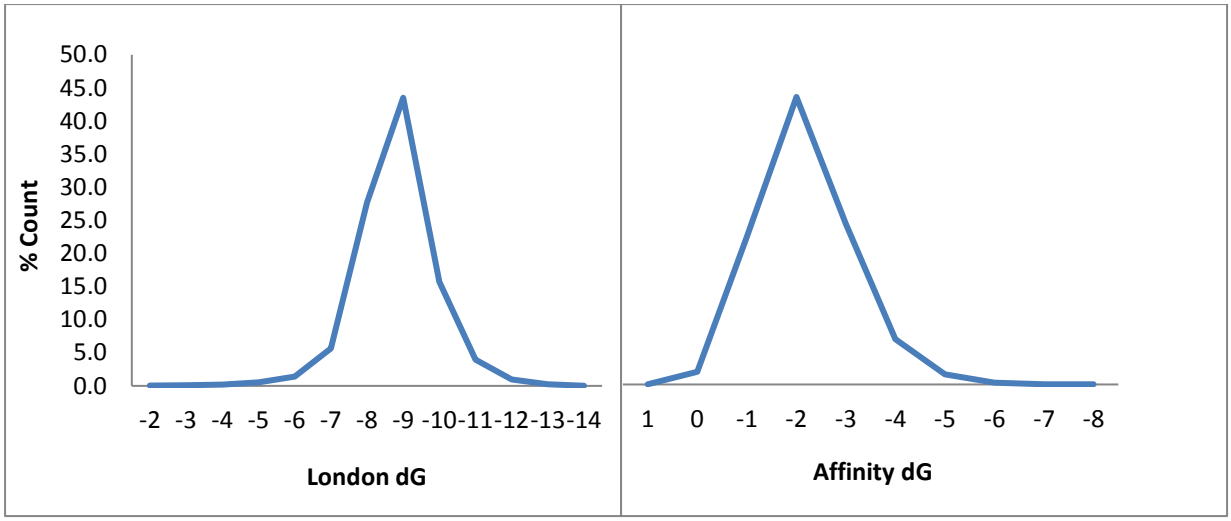

Fig.3. Distribution of the docking scores of the dataset towards the binding site of SARS-CoV-2 M^{pro}

15 drug molecules including Dobutamine, Mitoxantrone, Masoprocol, Tigecycline, Regadenoson, Neomycin, Gentamicin, Demeclocycline, Oxytetracycline, Chlotetracycline, Idarubicin, Streptomycin, Pentosan Polysulphate, Protokylol and Daunorubicin forming about 0.8% of the drug library gave ≥ 70% binding affinity to the active site of SARS-CoV-2 M^{pro} (as predicted by London dG and Affinity dG) compared to the re-docked native ligand and thus were selected as "the best scoring drugs" using the criteria already discussed. The ligand-protein interaction diagrams and the 2D structures of the drugs are shown in figure 4 and 5 respectively. Table 2a shows the description of the drugs, including the binding affinities of the best posed drugs. The molecular descriptors of the selected compounds as predicted by MOE software are shown in table 2b. Only Dobutamine, Masoprocol and Protokylol passed Pfizer rule of 5 for orally active drugs. Pharmacologically, Tigecycline, Demeclocycline, Oxytetracycline and Chlortetracycline belong to the tetracycline class of antibiotics; Neomycin, Gentamicin and Streptomycin belong to the class of aminoglycoside antibiotics; Idarubicin, Daunorubicin and Mitoxantrone belong to the anthracycline antileukemic drugs; Dobutamine and Protokylol belong to the β-adrenergic receptor agonist class of antihypertensive drugs; Masoprocol belong to the nordihydroguaiaretic acid class of antineoplastic drugs; Regadenoson belong to the Adenosine receptor agonist while Pentosan polysulfate belong to the class of semi-synthetic polysulphated xylan [26]. A common feature in Dobutamine, Masoprocol and Protokylol is the presence of catecholmethyl (3, 4-dihydroxybenzyl) moiety, which complies with the report that benzyl group contributes to hydrophobic grip of

inhibitors to M^{pro} active site [10]. Meanwhile, Mitoxantrone, Regadenoson, Idarubicin and Daunorubicin share the polycyclic hydrocarbon backbone of the tetracylines. Dobutamine, Misoprocol and Protokylol all have a similar structure related to the stilbenoids, except for Dobutamine and Protokylol where a Carbon atom is substituted by a Nitrogen atom in the hydrocarbon chain linking the aromatic rings. Among all the drugs, only Regadenoson has somewhat structural similarity to that of the cocrystallized inhibitor. A common structural feature relating Tigecycline, Demeclocycline, Oxytetracycline, Chlortetracycline and Regadenoson to the cocrystallized inhibitor is the presence of α-ketoamido group. This finding may be Iresponsible for the high and similarity in binding affinity observed with these drugs as several studies have shown that α-ketoamides are potent inhibitors of SARS-CoV-2 M^{pro} (5, 12). As structural analogs, Daunorubicin differs from Idarubicin only in the presence of a methoxy group at position 10 of the tetracene backbone. They both combine the structural features of the aminoglycosides and the tetracyclines, which may explain their relatively high and comparable binding affinities to the active site of the protease.

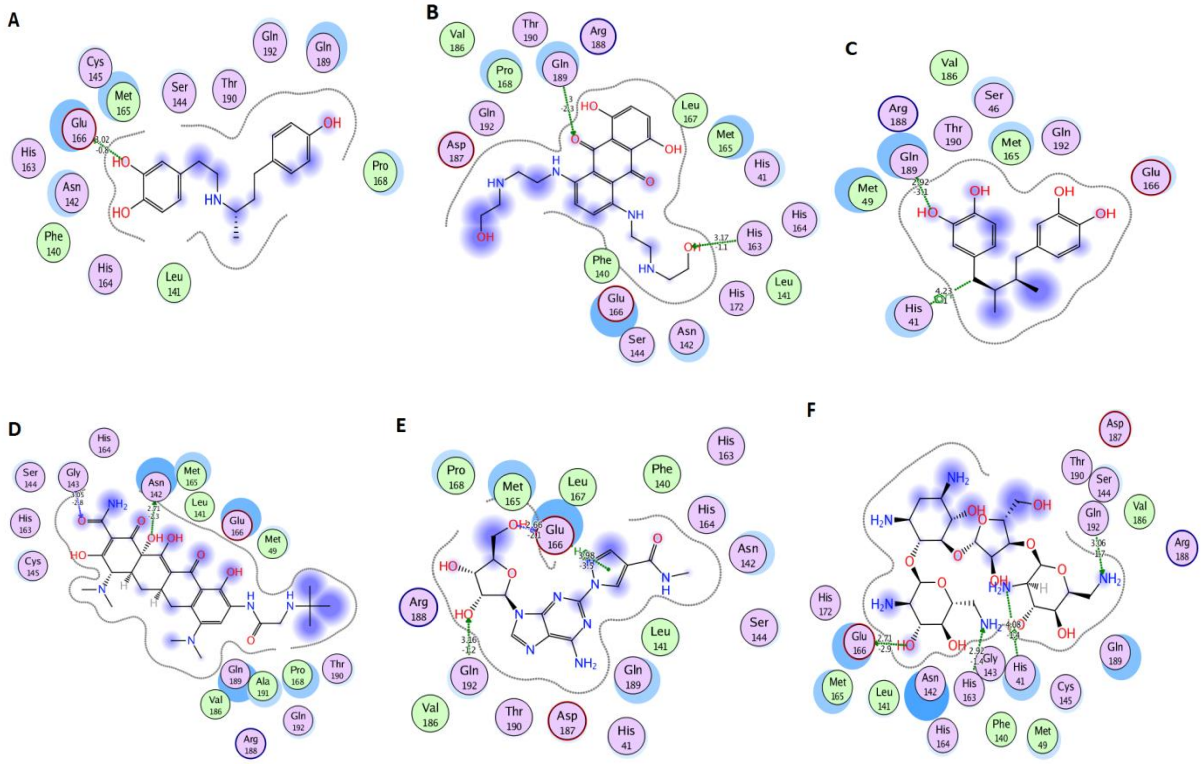

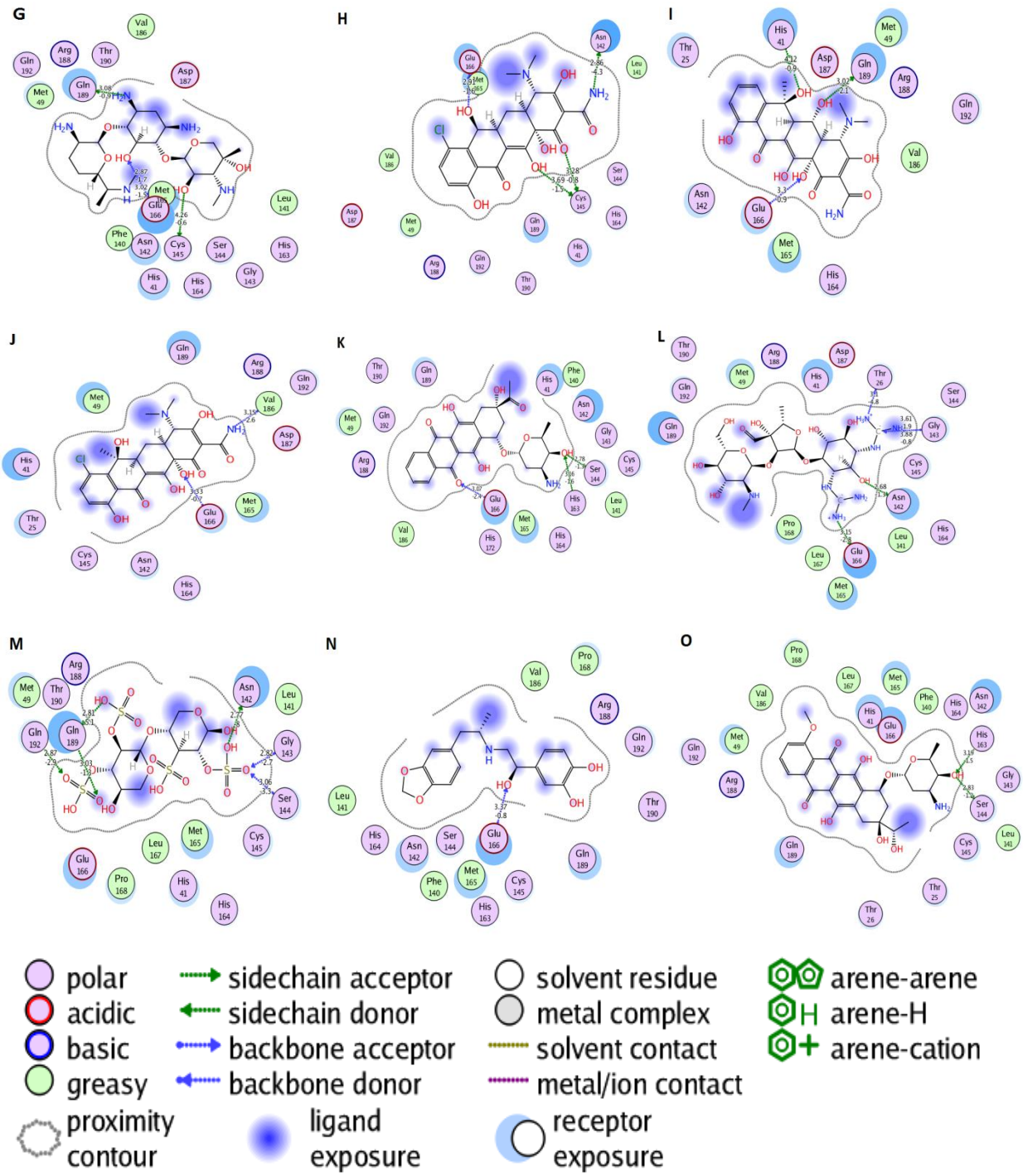

Fig.4. Ligand-protein interactions of "the best scoring drugs" as predicted by London dG and Affinity dG with least RMSDs (A) Dobutamine (B) Mitoxantrone (C) Masoprocol (D) Tigecycline (E) Regadenoson (F) Neomycin (G) Gentamicin (H) Demeclocycline (I) Oxytetracycline (J) Chlotetracycline (K) Idarubicin (L) Streptomycin (M) Pentosan Polysulphate (N) Protokylol (O) Daunorubicin

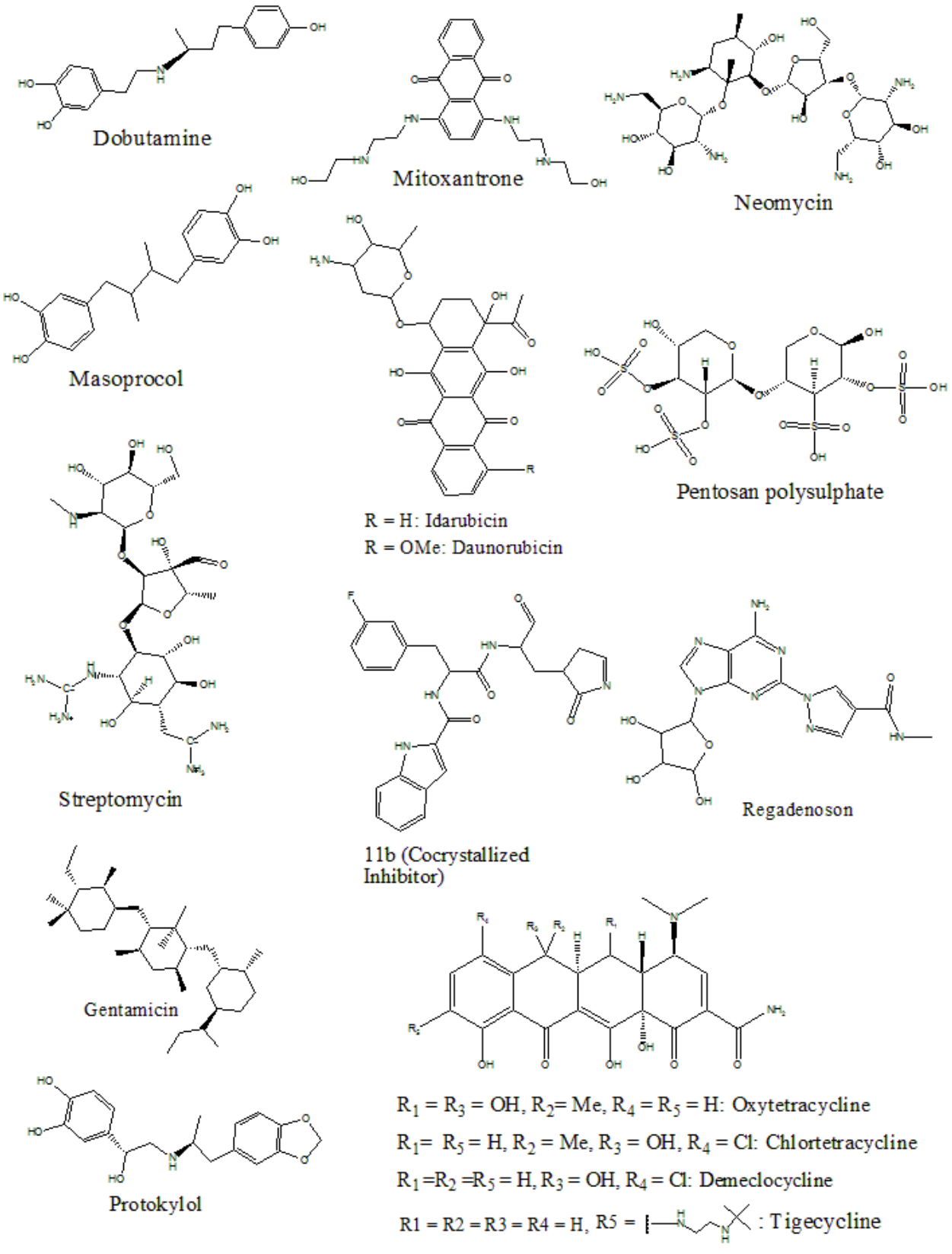

Fig.5. 2D Structures of 11b (cocrystallized inhibitor) and "the best scoring drugs"

Table 2a: Description of the best scoring drugs

Database Code	Drug Name	Chemical name	No. of best scoring poses	RMSD	Best Score	
					London dG	Affinity Dg
457	Dobutamine	(±)-4-[2-[[3-(4-Hydroxyphenyl)-1-methylpropyl]amino]ethyl]-1,2-benzenediol	3 of 10	1.4707	-12.3773	-3.7106
583	Mitoxantrone	1,4-Dihydroxy-5,8-bis({2-[(2-hydroxyethyl)amino]ethyl}amino)-9,10-anthraquinone	4 of 10	1.6071	-11.3407	-3.6808
656	Masoprocol	4-[(2R,3S)-4-(3,4-Dihydroxyphenyl)-2,3-dimethylbutyl]-1,2-benzenediol	5 of 10	1.2648	-12.6727	-3.5966
939	Tigecycline	(4S,4aS,5aR,12aS)-4,7-Bis(dimethylamino)-3,10,12,12a-tetrahydroxy-9-{[N-(2-methyl-2-propanyl)glycyl]amino}-1,11-dioxo-1,4,4a,5,5a,6,11,12a-octahydro-2-tetracenecarboxamide	3 of 10	1.2564	-11.3541	-4.9764
959	Regadenoson	2-[4-(Methylcarbamoyl)-1H-pyrazol-1-yl]adenosine	6 of 10	0.9437	-12.3320	-5.1407
968	Neomycin	(1R,2R,3S,4R,6S)-4,6-Diamino-2-{[3-O-(2,6-diamino-2,6-dideoxy-β-L-	4 of 10	1.9270	-12.5995	-5.7700

		idopyranosyl)-β-D-ribofuranosyl]oxy}-3-hydroxycyclohexyl 2,6-diamino-2,6-dideoxy-α-D-glucopyranoside				
969	Gentamicin	(1S,2S,3R,4S,6R)-4,6-Diamino-3-({(2R,3R,6S)-3-amino-6-[(1S)-1-(methylamino)ethyl]tetrahydro-2H-pyran-2-yl}oxy)-2-hydroxycyclohexyl 3-deoxy-4-C-methyl-3-(methylamino)-β-L-arabinopyranoside	3 of 10	1.2854	-13.2645	-6.7304
992	Demeclocycline	(4S,4aS,5aS,6S,12aS)-7-Chloro-4-(dimethylamino)-3,6,10,12,12a-pentahydroxy-1,11-dioxo-1,4,4a,5,5a,6,11,12a-octahydro-2-tetracenecarboxamide	4 of 10	1.5029	-11.5799	-4.0877
993	Oxytetracycline	(4S,4aR,5S,5aR,6S,12aS)-4-(Dimethylamino)-3,5,6,10,12,12a-hexahydroxy-6-methyl-1,11-dioxo-1,4,4a,5,5a,6,11,12a-octahydro-2-tetracenecarboxamide	3 of 10	1.7159	-12.6737	-3.2684
1002	Clotetracycline	(4S,4aS,5aS,6S,12aS)-7-Chloro-4-(dimethylamino)-3,6,10,12,12a-pentahydroxy-6-methyl-1,11-dioxo-	4 of 10	1.7895	-11.5523	-3.5106

		1,4,4a,5,5a,6,11,12a-octahydro-2-tetracenecarboxamide				
1050	Idarubicin	(1S,3S)-3-Acetyl-3,5,12-trihydroxy-6,11-dioxo-1,2,3,4,6,11-hexahydro-1-tetracenyl 3-amino-2,3,6-trideoxy-α-L-lyxo-hexopyranoside	6 of 10	1.3183	-11.9944	-6.7335
1074	Streptomycin	1,1'-[(1R,2R,3S,4R,5R,6S)-4-({5-Deoxy-2-O-[2-deoxy-2-(methylamino)-α-L-glucopyranosyl]-3-C-formyl-α-L-lyxofuranosyl}oxy)-2,5,6-trihydroxy-1,3-cyclohexanediyl]diguanidine	4 of 10	2.8328	-11.5010	-4.2953
1258	Pentosan Polysulphate*	(2S, 3R, 4S, 5R)-5-hydroxy-2-{[(3R, 4S, 5R, 6R)-6-hydroxy-4,5-bis(sulfooxy)oxan-3-yl]oxy}-4-(sulfooxy)oxan-3-yl]oxidanesulfonic acid	8 0f 10	1.2728	-13.1774	-3.5412
1331	Protokylol	4-(2-{[1-(1,3-Benzodioxol-5-yl)-2-propanyl]amino}-1-hydroxyethyl)-1,2-benzenediol	4 of 10	1.8631	-12.7550	-8.0873
1636	Daunorubicin	(1S,3S)-3-Acetyl-3,5,12-trihydroxy-10-methoxy-6,11-dioxo-1,2,3,4,6,11-hexahydro-1-tetracenyl 3-amino-2,3,6-trideoxy-α-L-lyxo-hexopyranoside	3 of 10	1.3695	-13.0013	-3.9401

Chemical names were obtained from ChemSpider (http://www.chemspider.com/). * Chemical name was obtained from PubChem (https://www.pubchem.ncbi.nlm.nih.gov/).

Table 2b: Molecular descriptors of the best scoring drugs

Database ID	Drug Name	Molecular weight (Da)	LogP (o/w)	No. of hydrogen bond donors	No. of hydrogen bond acceptors	Pfizer Violation
457	Dobutamine	301.3860	3.6660	4	4	0
583	Mitoxantrone	444.4880	-0.5360	8	10	1
656	Masoprocol	302.3700	4.4800	4	4	0
939	Tigecycline	585.6580	-0.2560	8	13	3
959	Regadenoson	390.3600	-2.6329	6	13	2
968	Neomycin	614.6500	-9.2403	19	19	3
969	Gentamicin	477.6030	-2.9050	11	12	2
992	Demeclocycline	464.8580	-0.2590	7	10	1
993	Oxytetracycline	460.4390	-1.4570	8	11	2
1002	Clotetracycline	478.8850	0.1480	7	10	1
1050	Idarubicin	497.5000	1.3730	6	10	1
1074	Streptomycin	543.5250	0.5070	7	12	3
1258	Pentosan Polysulphate	586.4980	-5.5605	6	20	3
1331	Protokylol	331.3680	2.5760	4	6	0
1636	Daunorubicin	529.5420	1.4140	7	11	3

Table 3: Main pharmacological features of the best scoring drugs as predicted by London dG and Affinity dG

Drug name	Status	Mechanism	Indication	Adverse Effects/Toxicity
Dobutamine	Approved	B1-adrenergic agonist. Does not evoke	Short-term treatment of heart failure	

		vasoconstriction or tachycardia		
Mitoxantrone	Approved, Investigational	Intercalates DNA through H-bonding causing crosslinks and strand breaks	Treatment of chronic, relapsing multiple sclerosis	Severe leukopenia with infection
Masoprocol	Approved, Investigational	Potent 5-lipooxygenase inhibitor	Treatment of actinic keratoses	Symptoms of overdose or allergic reaction include bluish coloration of skin, dizziness, feeling faint, trouble breathing
Tigecycline	Approved	Inhibits protein synthesis in bacteria by binding to 30s ribosomal subunit and blocking entry of amino-acyl tRNA molecule into the A site of the ribosome	Antibiotic	Nausea/vomiting, headache, photosensitivity, discoloration of growing teeth, and fetal damage
Regadenoson	Approved, Investigational	A2A receptor agonist	Diagnostic agent for radionuclide myocardial perfusion imaging (MPI)	Dyspnea, headache, flushing, chest discomfort, dizziness, angina pectoris, and nausea
Neomycin	Approved	Inhibits bacterial ribosomes by binding to the	Broad-spectrum antibiotic	Neurotoxicity, ototoxicity and/or nephrotoxicity.

		30S ribosomal subunit of susceptible bacteria and disrupting protein synthesis		May cause fetal harm and total irreversible bilateral congenital deafness when administered in pregnant women
Gentamicin	Approved	The same as Neomycin	The same as Neomycin	The same as Neomycin
Demeclocycline	Approved	The same as Tigecycline	The same as Tigecycline	The same as Tigecycline
Oxytetracycline	Approved, Investigational, Vet approved	The same as Tigecycline	The same as Tigecycline	The same as Tigecycline
Chlortetracycline	Approved, Investigational, Vet approved	The same as Tigecycline	The same as Tigecycline	The same as Tigecycline
Idarubicin*	Approved	Antimitotic and cytotoxic activity	Treatment of acute myeloid leukemia (AML) in adults	
Streptomycin	Approved, Vet approved	The same as Neomycin	The same as Neomycin (For the treatment of tuberculosis)	The same as Neomycin
Pentosan Polysufate*	Approved	Binds fibroblast growth factors (FGFs) as well as other heparin-binding growth factors	Relief of bladder pain or discomfort associated with intestinal cystitis	
Protokylol*	Approved, Vet approved	β-adrenergic receptor agonist	Bronchodilator[1]	

Daunorubicin	Approved	DNA intercalation and inhibition of topoisomerase II activity	Remission induction in acute nonlymphocytic leukemia of adults

Data were obtained from DrugBank (https://www.drugbank.ca). *Missing data are not available on DrugBank. [1]Data obtained from Swiss Pharmaceutical Society. Index Nominum 2000: International Drug Directory.

We went further to discuss the notable ligand-protein interactions observed with "the best scoring drugs" using the interactions observed in the cocrystallized inhibitor 11b (positive control) and those reported in literature as reference standard for comparison and drawing of inferences.

Dobutamine and Protokylol are β-adrenergic agonist catecholamines. Dobutamine has predominantly β1 selectivity and is thus used for the short-term treatment of patient with cardiac decompensation due to depressed contractility of the cardiac muscles (heart failure). It has a therapeutic advantage of not evoking vasoconstriction or tachycardia. On the other hand, Protokylol is selective for β2 and is used mainly as a bronchodilator (see table 3). The Dobutamine-SARS-CoV-2 M^{pro} interaction diagram is shown in figure 4A. 3 out of the 10 conformations generated were retained (as previously discussed under the selection criteria) of which the best posed conformation with the least RMSD of 1.4707 Å had binding affinities of -12.3773 Kcal/mol and -3.7106 Kcal/mol for London dG and Affinity dG, respectively (see table 2a). From figure 4A, the 2-hydroxyl group of the catechol moiety donated 3.03-Å H-bond to the Glu166 residue, stabilizing the complex formed. Since ligand-protein interaction involving H-bond formation with Glu166 residue has been reported to play a role in binding and stabilizing of ligands towards the binding pocket of M^{pro} thus, this interaction is considered important [22]. If this trend continues, we may then infer that the catechol moiety may be important for binding of inhibitors to SARS-CoV-2 M^{pro}. The best posed conformation of Protokylol had binding affinity scores of -12.7550 Kcal/mol and -8.0873 Kcal/mol according to London dG and Affinity dG respectively with RMSD of 1.8631 Å. Figure 4N shows the ligand-protein interaction of Protokylol and SARS-CoV-2 M^{pro} in which Glu166 donated 3.37-Å H-bond to the 1-hydroxyl group. But surprisingly, the Affinity dG score for Protokylol was the best recorded among the 15 selected drug molecules (see table 2a)

even though only one ligand-protein interaction was observed. A possible explanation for this observation could be in the orientation of the molecule towards the binding pocket of SARS-CoV-2 M^{pro} which reduces repulsion and steric hindrances and the fact that the molecule has polar functional groups surrounded by polar amino acid residues.

Masoprocol is a potent lipoxygenase inhibitor that interferes with arachidonic acid metabolic pathway. It also inhibits formyltetrahydrofolate synthetase. It is used for the treatment of actinic keratosis (see table 3). This drug was withdrawn from the United States market in June 1996 [26], our goal in this work however, is not to reposition it for COVID-19 treatment but to seek for structural and pharmacophoric features that may lead to the development of better drugs. Figure 4C shows the interaction diagram with the amino acid residues present on the active site of SARS-CoV-2 M^{pro}. 5 conformations out of the 10 runs performed exhibited comparable binding affinity to that of the re-docked native ligand (see table 2a). Masoprocol exhibited some very classical ligand-protein interactions with the amino acid residues present in active site of M^{pro}. Of particular importance is the 4.23-Å π-hydrogen interaction between His41 of the catalytic dyad and the α-Hydrogen of the butane backbone. This interaction supports the finding that arene-hydrogen interaction between His41 and benzyl group is essential for potent SARS-CoV-2 M^{pro} inhibitory effect [5, 12]. The Oxygen atom of the 2-hydroxyl group of the catechol moiety also donated 2.92-Å H-bond to Gln189 resulting in a binding affinity of -12.6727 Kcal/mol for London dG and -3.5966 Kcal/mol for Affinity dG, with RMSD of 1.2648 Å. A similar ligand-interaction was observed with Dobutamine-SARS-CoV-2 M^{pro} complex. However, for Dobutamine, the Oxygen atom of the 2-hydroxyl group donated H-bond to Glu166, which lies on the opposite side of Gln189 residue. But since Glu166 and Gln189 residues are both essential for the viral replication, these interactions are also considered top-notch. The structural similarity of Dobutamine, and Masoprocol could be responsible for this observation.

Mitoxantrone is an anthracenedione-derived antineoplastic agent used for the treatment of chronic, progressive or worsening multiple sclerosis. It works by intercalating DNA via hydrogen bonding causing crosslinks and stand breaks (see table 3). 4 conformations out of the 10 runs performed exhibited comparable binding affinity to that of the re-docked native ligand (see table 2a). The following ligand-protein interactions as shown in figure 4B were observed between Mitoxantrone and SARS-CoV-2 M^{pro}. Gln189 donated 3.0-Å H-bond to the 5-oxo group and His163 donated 3.17-Å H-bond to the hydroxyl group of the side chain stabilizing the ligand-protein complex

formed. This pose had a binding affinity of -11.3407 Kcal/mol and -3.6808 Kcal/mol as predicted by London dG and Affinity dG respectively with RMSD of 1.6071 Å. This observation buttresses the study that ligand to protein H-bond interactions involving Gly143, His163, and Glu166, the three polar amino acid residues present in the active site of M^{pro} are critical in the high affinity binding of inhibitors [24]. Again, a Gln residue is almost always required in the binding of substrate to binding pocket of M^{pro} [5]. Thus, high binding affinity of ligands to Gln residues (such as Gln189) is essential in preventing this substrate binding and therefore handcuffing the substrate assembly cascade necessary for the survival of the virus.

Tigecycline, Demeclocycline, Oxytetracycline, and Chlortetracycline belong to the broad-spectrum tetracycline class of antibiotic that inhibit protein synthesis in susceptible bacteria by binding to 30s ribosomal subunit and blocking entry of amino-acyl tRNA molecule into the A site of the ribosome (see table 3). The common structural nucleus of the tetracycline class of drugs is the presence of (4S, 4aR, 5aR, 12aS)-4-(dimethylamino)-10, 12, 12a- trihydroxy-1, 11-dioxo-1, 4, 4a, 5, 5a, 6, 11, 12a-octahydro-2-tetracenecarboxamide, which forms the structural scaffold of the tetracyclines. The best posed conformation of Tigecycline exhibited binding affinities (as predicted by London dG and Affinity dG) of -12.6727 Kcal/mol and -3.5966 Kcal/mol respectively with RSMD of 1.2564 Å (see table 2a). From figure 4D, the Oxygen atom of the 2-carboxamide group in Tigecycline accepted 3.05-Å H-bond from Gly143. The Asn142 accepted 2.71-Å H-bond from the 12a-hydroxyl group of Tigecycline. The binding affinity scores of the best posed conformation of Demeclocycline with RMSD 1.5029 Å according to London dG and Affinity dG were -11.5799 Kcal/mol and -4.0877 Kcal/mol respectively (see table 2a). The following ligand-protein interactions were observed between Demeclocycline and SARS-CoV-2 M^{pro}. The 6-hydroxyl group donated 2.91-Å H-bond to Glu166. Asn142 residue accepted 2.86-Å H-bond from the amino group of the 2-carboxamide moiety. The Cys145 residue of the catalytic dyad accepted 3.69/3.28-Å H-bonds from the 12-hydroxyl and the 1-oxo groups respectively. Oxytetracycline exhibited unique ligand-protein interactions, the best posed conformation had RMSD of 1.7159 Å with docking scores of -12.6737 Kcal/mol and -3.2684 Kcal/mol according to the two scoring functions used (see table 2a). A 4.12-Å π-hydrogen bond was observed between the Hydrogen atom of the 6-hydroxyl group of Oxytetracycline and His41 residue of the catalytic dyad. A similar interaction was observed in the cocrystallized ligand (see figure 2) and has been reported in literature to be essential for inhibitory binding of ligands to the active site of M^{pro} [22]. The 5-hydroxyl group of

Oxytetracycline donated 3.02-Å H-bond to Gln189. While the 12a-hydroxyl group also donated 3.30-Å H-bond to Glu166 (see figure 4I). Chlortetracycline and Oxytetracycline share a very similar structure, differing only in presence and/or absence of chloro group and hydroxyl group at position 6 and position 7 of the tetracene backbone (see figure 5). The best posed structure of Chlortetracycline had RMSD of 1.7895 Å and the binding affinity scores of -11.5523 Kcal/mol and -3.5106 Kcal/mol according to London dG and Affinity dG scoring functions respectively (see table 2a). The 12a-hydroxyl group of Chlortetracycline donated 3.33-Å H-bond to Glu166. This interaction was seen in Oxytetracycline and perhaps, the very close structural similarity between the two drug molecules accounted for this common observation. Additionally, the Val186 residue of Chlortetracycline accepted 3.15-Å H-bond from the amino group of the 2-carboxamide moiety (see figure 4J).

Neomycin, Gentamicin and Streptomycin belong to the class of aminoglycoside antibiotic. They inhibit bacterial ribosomes by binding to the 30S ribosomal subunit of susceptible bacteria and disrupting protein synthesis. As broad spectrum antibiotic, they are used for the treatment of various bacterial infections (see table 3). The common structural features among these drugs are the presence of polyhydroxylated cyclohexane moiety and amino sugars in the form of arabinofuranose and/or arabinopyranose. The best posed structure of Neomycin exhibited high binding affinities of -12.5995 Kcal/mol and -5.7700 Kcal/mol according to London dG and Affinity dG respectively towards the binding pocket of SARS-CoV-2 M^{pro} (see table 2a). Neomycin-SARS-CoV-2 M^{pro} complex is shown in figure 4F, in which His163 donated 2.92-Å H-bond to the 6-amino group of the 2, 6-dideoxy-α-D-glucopyranosyl moiety. The 2-amino group of the 2, 6-dideoxy-β-L-idopyranosyl moiety interacted with the His41 residue of the catalytic dyad via 4.08-Å π-hydrogen bonding. A similar ligand-protein interaction was observed in the cocrystallized inhibitor though a benzyl rather than an amino hydrogen atom was involved in the arene-hydrogen bonding (see figure 2). The 3-hydroxyl group of 2, 6-dideoxy-α-D-glucopyranosyl moiety donated 2.71-Å H-bond to the glu166 residue. A similar interaction was also seen in the cocrystallized inhibitor. Lastly, the 6-amino group of the 2, 6-dideoxy-β-L-idopyranosyl moiety accepted 3.06-Å H-bond from the Gln192 residue. However, this interaction was not seen in the cocrystallized inhibitor. The best posed conformation of Gentamicin with RMSD of 1.2854 Å also exhibited high ligand-protein interactions similar to that of Neomycin, with binding affinity scores of -13.2645 Kcal/mol and -6.7304 Kcal/mol according to London dG and Affinity dG respectively (see table

2a). Figure 4G shows the binding mode and ligand-protein interactions of Gentamicin towards the active site of SARS-CoV-2 M^{pro}. The 2-hydroxyl group of the 3-deoxy-β-L-arabinopyranosyl moiety donated 4.26-Å H-bond to the Cys145 of the catalytic dyad. The Glu166 residue accepted/donated 2.87/3.02-Å H-bonds respectively to the 2-hydroxyl group of the cyclohexyl moiety. The 6-amino group of the cyclohexyl moiety donated 3.08-Å H-bond to the Gln189 residue. Though, a similar interaction was not seen in the cocrystallized ligand, but ligand protein interaction involving Gln189 has been reported in literature to enhance ligand binding to M^{pro} [5]. Most of the ligand-protein interactions seen in Streptomycin involved the guanidine moiety and the 2-hydroxyl group of the cyclohexyl moiety donating/accepting H-bonds from Glu166, Asn142, Gly143, and Thr26 (see figure 4L). The Glu166 residue accepted 3.15-Å H-bond from the protonated amino group of the 1-guanidine moiety. The 2-hydroxyl group of the cyclohexyl moiety donated 2.68-Å H-bond to the Asn142 residue. The protonated amino group of the 3-guanidine moiety donated 3.10-Å H-bond to the Thr26 residue, while the carbanion of the same moiety accepted 3.61/3.88-Å H-bonds from Gly143 residue. These ligand-protein interactions resulting from the best posed conformation of Streptomycin had affinity binding scores of -11.5010 Kcal/mol and -4.2953 Kcal/mol according to London dG and Affinity dG respectively with RMSD of 2.8328 Å. Among the best posed structures of the 15 selected drug molecules, Streptomycin exhibited the highest RMSD (see table 2a).

Regadenoson is an A2A adenosine receptor agonist that causes coronary vasodilation and used for myocardial imaging though, it is still investigational (see table 3). The best posed conformation of Regadenoson had the lowest RMSD of 0.9437 Å with affinity binding energies of -12.3320 Kcal/mol and -5.1407 Kcal/mol as estimated by London dG and Affinity dG respectively (see table 2a). Figure 4E shows Regadenoson-SARS-CoV-2 M^{pro} complex in which the Glu166 residue accepted 2.66-Å H-bond from the 5-hydroxyl group of the 1-deoxy-β-D-ribofuranose moiety and shared a 3.98-Å π-hydrogen bond with the 4-(methylcarbamoyl)-1H-pyrazol moiety. Also, the 2-hydroxyl group of the 1-deoxy-β-D-ribofuranose moiety accepted 3.16-Å H-bond from Gln192 residue.

Idarubicin and Daunorubicin are orally administered anthracycline antineoplastic with antimitotic and cytotoxic activity, used for the treatment of acute myeloid leukemia (AML). They works by intercalating base pairs in DNA strands (see table 3). Both drug molecules had very similar binding affinities and ligand-protein interactions with very slight discrepancies. The best posed structure

of Idarubicin had affinity binding scores of -11.9944 Kcal/mol and -6.7335 Kcal/mol respectively for London dG and Affinity dG respectively with RMSD of 1.3183 Å (see table 2a). From the ligand-protein interaction diagram shown in figure 4K, the 4-hydroxyl group of the 2, 3, 6-trideoxy-α-L-lysohexopyranosyl moiety donated/accepted 2.78/3.16-Å H-bonds from the Ser144 and His163 residues respectively. The Glu166 residue of the active site also donated 3.07-Å H-bond to the 11-oxo group of the tetracene backbone. However, the only ligand-protein interaction lacking in Daunorubicin is that involving the 11-oxo group and the Glu166 residue (see figure 4O). The best fitted structure of Daunorubicin to the active site of M^{pro} had affinity binding energies of -13.0013 Kcal/mol and -3.9401 Kcal/mol as predicted by London dG and Affinity dG respectively with RMSD of 1.3695 Å (see table 2a), which is very close to that of Idarubicin. This consistency observed with the binding modes of structural analogs towards the binding pocket of Mpro reinforces the search for common structural scaffold which this work is all about.

Pentosan polysulfate is a sulfated pentosyl polysaccharide with heparin-like properties used for the relief of bladder pain or discomfort associated with interstitial cystitis (see table 3). The best posed conformation of Pentosan polysulfate towards the binding pocket of M^{pro} had binding affinity scores of -13.1774 Kcal/mol and -3.5412 Kcal/mol according to London dG and Affinity dG respectively with RMSD of 1.2728 Å (see table 2a). Pentosan polysulfate exhibited a number of ligand-protein interactions involving mainly the sulfate groups and the Gln192, Gln189, Asn142, Gly143 and Ser144 residues of the active site which as expected are all polar interactions. The oxygen atom of the 4-sulfoxy moiety accepted 2.82/3.06-Å H-bonds from Gly143 and Ser144 residues respectively. Whereas, the hydroxyl group of the same moiety donated 2.77-Å H-bond to the Asn142 residue. At the other end of the molecule, the Gln189 residue accepted/donated H-bonds from/to the hydroxyl group of the 4'-sulfoxy and the oxygen atom of the 3'-sulfoxy moieties respectively. Also, the Gln192 residue donated 2.87-Å H-bond to the oxygen atom of the 3'-sulfoxy moiety.

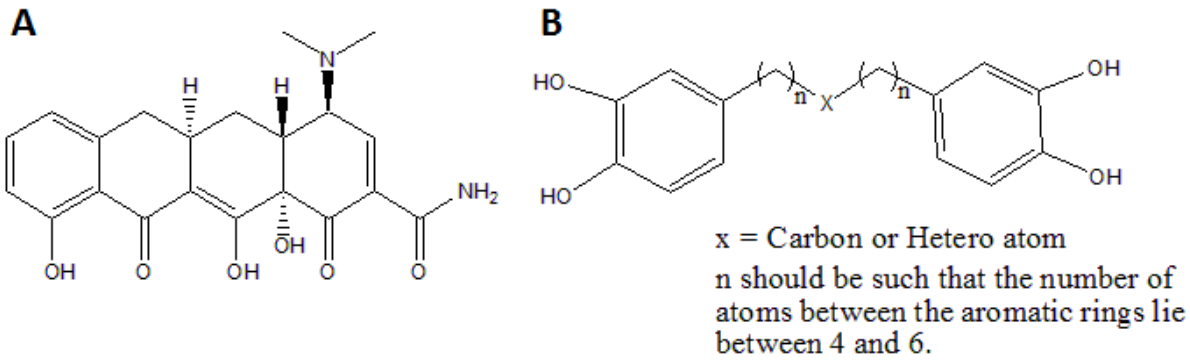

Fig.6. Structural Scaffolds identified to bind to SARS-CoV-2 M^{pro} active site. (A): The common structural nucleus of the tetracyclines, (4S,4aR,5aR,12aS)-4-(dimethylamino)-10,12,12a-trihydroxy-1,11-dioxo-1,4,4a,5,5a,6,11,12a-octahydro-2-tetracenecarboxamide. (B): The stilbenoid-like structure common to Dobutamine, Protokylol and Masoprocol

The presence of α-ketoamido functionality in the common structural nucleus of the tetracyclines may justify the high binding affinity of these drugs towards SARS-CoV-2 M^{pro}. Thus, (4S,4aR,5aR,12aS)-4-(dimethylamino)-10,12,12a-trihydroxy-1,11-dioxo-1,4,4a,5,5a,6,11,12aoctahydro-2-tetracenecarboxamide (see figure 6A) could be considered a starting point for the design of drugs with potent SARS-CoV-2 M^{pro} inhibitory effect with the tetracene nucleus playing a role in the proper orientation of the molecule toward the protease binding pocket while the array of electron donators/acceptors on it interact with the active site amino acid residues. The common structural nucleus of Dobutamine, Protokylol and Masoprocol can be approximated to a stilbenoid-like structure in which the number of atoms between the two aromatic rings lies between 4 and 6 (see figure 6B). Arabinofuranose, arabinopyranose, their amino-substituted equivalents, sulfate, catechol, benzyl, guanidine, and polyhydroxylated/polyaminated cyclohexane moieties all participated in the binding of "the best scoring drug molecules" to the active site of SARS-CoV-2 M^{pro}.

3. EXPERIMENTAL

3.1. Drug Library Description and Preparation

The 3-dimensional chemical structures of 1852 drugs approved by the FDA between 1939 and 2018 forming the study dataset were retrieved from the database e-Drug3D [17] and prepared for molecular simulation purpose. In order to determine the Pfizer's rule of 5 for the used compounds

dataset, the molecular weight, lipophilicity, the number of hydrogen bond donors and acceptors were calculated using MOE software [18]. The Pfizer's rule of 5 states that, in general, an orally active drug has no more than one violation of the following criteria: 1. No more than 5 hydrogen bond donors 2. No more than 10 hydrogen bond acceptors 3. A molecular mass less than 500 Daltons and 4. Octanol-water-partition coefficient (logP) less than 5 [27, 28].

3.2. Treatment of the X-ray Crystal Structure of M^{pro}

The X-ray crystal structure of M^{pro} in complex with an inhibitor 11b with PDB code 6M0K and resolution 1.50 Å was retrieved from the protein databank [18]. The protein− ligand complex was treated as follows; the complex was treated using MOE software [19]. The cocrystallized water molecules, small molecules and nonessential ions such as sodium, sulfate and phosphate ions were deleted. The retained protein−ligand complex was protonated using the protonate 3D procedure implemented in MOE [19].The protonated complex was then energy minimized in order to remove atomic clashes, using the Merck Molecular (MMFF94) Force field [20] until a gradient of 0.001 kcal/mol was attained. The docking of all compounds toward the binding site of M^{pro} was carried out using the MOE Dock tool.

3.3. Validation of the Docking Protocol

The docking protocol was validated by re-docking the cocrystallized native ligand into the active site of M^{pro} in different grid boxes dimensions using London dG and Affinity dG implemented in MOE software [19]. After several trials, the grid box dimensions in x-, y- and z-axes for both origin and radius which gave the best fit with the cocrystallized ligand with least root-mean-square-deviation (RMSD) less than 3Å was retained and used for the study. This is because RMSD less than 3 Å shows that the protein did not undergo large conformational changes during the molecular docking indicating stability of the ligand-protein complex formed. Docking validation was an attempt to identify the best docking parameters which reproduces the ligand conformation (docking poses) within the binding pocket, i.e., having the lowest RMSD values, with respect to the experimental binding mode (X-ray crystal structure).

3.4. Virtual screening

After the validation of the docking protocol and scoring predictability with the cocrystallized ligand (positive control), virtual screening of the drug library was performed by docking the drug library towards the active site of M^{pro} using the same docking programs in MOE and maintaining the methods, grid box centroids and dimensions obtained in the validation phase. Three main stages

were involved in the docking process: Conformational Analysis of ligands, Placement, and Scoring. In the ligand Conformational Analysis stage, conformations from a single 3D conformation input ligand were generated by conducting a systematic search methodology. All combinations of angles were created for each ligand. During the Placement stage, a collection of poses was generated from the pool of ligand conformations using the Triangle Matcher placement method. At the Scoring stage, the poses generated during the Placement stage were scored using two scoring methods: London dG and Affinity dG, all implemented in MOE.

3.5. Selection of "the best scoring drugs"

A total of 10 runs were done for each drug molecule of the database from which the best scoring drugs with least RMSD were selected as follows: Firstly, any drug molecule in which at least 3 out of the 10 poses have affinity high binding modes predicted simultaneously by London dG and Affinity dG to be ≥ 70% of that of the best pose of the re-docked cocrystallized ligand with least RMSD were retained. Secondly, from the retained molecules, those that made at least one ligand-protein interactions similar to those observed with the cocrystallized ligand were considered as "the best scoring drugs".

3.6. Selection of the common structural scaffolds

Among "the best scoring drugs", structural nucleus common to drug molecules that made at least one ligand-protein interaction with the key amino acid residues including His41, Cys145, Glu166 and other amino acid residues present at the active site of SARS-CoV-2 M^{pro}, which have been reported in previous work to be essential for binding of inhibitors to the protease active site [21 – 24] were selected.

4. CONCLUSION

We have been able to identify two structural scaffolds: (4S, 4aR, 5aR, 12aS)-4-(dimethylamino)-10, 12, 12a- trihydroxy-1, 11-dioxo-1, 4, 4a, 5, 5a, 6, 11, 12a-octahydro-2-tetracenecarboxamide and the stilbenoid-like structure from drug molecules which could strongly bind to SARS-CoV-2 M^{pro} and thus can serve as starting point in the design of drugs with anti-SARS-CoV-2 M^{pro} activity. The fact that these structural nuclei are well characterized and are derived from FDA approved drug molecules can greatly reduce the risk of attrition during structure-based drug design.

AUTHOR CONTRIBUTIONS: E.O. conceived and plan ned the experiments. E.O. prepared the library and performed the docking analyzes. E.O. and I.C.U. analyzed the intermolecular interactions between M^{pro} and inhibitor and the best scoring drugs. E.O. and S.N. performed the validation of the VS with the SARS-CoV-2 M^{pro} cocrystallized inhibitor. E.O., U.J.E. and H.C.E. prepared the figures and tables. E.O., I.K.E. and S.K.M. wrote the manuscript. A.A.E. and O.O. collected data on SARS-CoV-2 Mpro and proofread the manuscript. E.O. coordinated all the study. All the authors have read and agreed to the published version of the manuscript.

FUNDING: This research received no external funding.

ACKNOWLEDGEMENTS: We thank the Online Cheminformatics - CNRS for providing us access to use their e-Drug3D library. The Chemical Computing Group is also acknowledged for the academic license to use the Molecular Operating Environment (MOE) Software.

CONFLICT OF INTERESTS: The authors declare no conflict of interest.

REFERENCES

[1] Zhu N, Zhang D, Wang W, Li X, Yang B, Song J, Zhao X, Huang B, Shi W, Lu R, Niu P, Zhan F, Ma, X, Wang D, Xu W, Wu G, Gao G F, Tan W. A Novel Coronavirus from Patients with Pneumonia in China, 2019. *N. Engl. J. Med.* 2020, 382, 727-733, doi: 10.1056/NEJMoa2001017.

[2] World Health Organization. Novel Coronavirus (2019-nCoV) Situation Reports; World Health Organization, Geneva, Switzerland, 2020.

[3] Cao B, Wang Y, Wen D, Liu W, Wang J, Fan G, Ruan L, Song B, Cai Y, Wei M, Li X, Xia J, Chen N, Xiang J, Yu T, Bai T, Xie X, Zhang L, Li C, Yuan Y, Chen H, Li H, Huang H, Tu S, Gong F, Liu Y, Wei Y, Dong C, Zhou F, Gu X, Xu J, Liu Z, Zhang Y, Li H, Shang L, Wang K, Li K, Zhou X, Dong X, Qu Z, Lu S, Hu X, Ruan S, Luo S, Wu J, Peng L, Cheng F, Pan L, Zou J, Jia C, Wang J, Liu X, Wang S, Wu X, Ge Q, He J, Zhan H, Qiu F, Guo L, Huang C, Jaki T, Hayden F G, Horby P W, Zhang D, Wang C. A Trial of Lopinavir-Ritonavir in Adults Hospitalized with Severe Covid-19. *N. Engl. J. Med*. 2020, 382, 1787-1799, doi: 10.1056/NEJMoa2001282.

[4] Gorbalenya A E, Baker S C, Baric R S, de Groot R J, Drosten C, Gulyaeva A A, Haagmans B L, Lauber C, Leontovich A M, Neuman B W, Penzar D, Perlman S, Poon L L M, Samborskiy D,

Sidorov I A, Sola I, Ziebuhr J. Severe acute respiratory syndrome-related coronavirus: The species and its viruses - a statement of the Coronavirus Study Group. *bioRxiv* 2020.02.07.937862 [preprint]. 11 February 2020, doi: 10.1038/s41564-020-0695-z.

[5] Dai W, Zhang B, Su H, Li J, Zhao Y, Xie X, Jin Z, Liu F, Li C, Li Y, Bai F, Wang H, Cheng X, Cen X, Hu S, Yang X, Wang J, Liu X Xiao G, Jiang H, Rao Z, Zhang L K, Xu Y, Yang H, Liu H. Structure-based design of antiviral drug candidates targeting the SARSCoV-2 main protease, *Science* 2020, doi: 10.1126/science.abb4489.

[6] Kandeel M, Al-Nazawi M. Virtual screening and repurposing of FDA approved drugs against COVID-19 main protease, *Life Sci*, 2020, 251, 117627, doi: 10.1016/j.1fs.2020.117627.

[7] Xu X, Han M, Li T, Sun W, Wang D, Fu B, Zheng X, Yang Y, Li X, Zhang X, *et al*. Effective Treatment of Severe COVID-19 Patients with Tocilizumab. Proc. Natl. Acad. Sci. USA 2020, 117, 10970-10975, doi: 10.1073/pnas.2005615117.

[8] Wang M, Cao R, Zhang L, Yang X, Liu J, Xu M, Shi Z, Hu Z, Zhong W, Xiao G. Remdesivir and chloroquine effectively inhibit the recently emerged novel coronavirus (2019-nCoV) in vitro. *Cell Res*. 2020, 30, 269 – 271, doi: 10.1038/s41422-020-0282-0.

[9] Ullrich S, Nitsche C. The SARS-CoV-2 main protease as drug target. *Bioorganic & Medicinal Chemistry Letters*, 2020, 30, 127377. doi: 10.1016/j.bmcl.2020.127377.

[10] Gimeno A, Mestres-Truyol J, Ojeda-Montes M J, Macip G, Saldivar-Espinoza B, Cereto-Massague A, Pujadas G, Garcia-Vallve S. Prediction of novel inhibitors of the main protease (M-pro) of SARS-CoV-2 through consensus docking and drug reposition. *Int. J. Mol. Sci.* 2020, 21, 3793, doi: 10.3390/ijms21113793.

[11] Ren Z, Yan, L, Zhang N, Guo Y, Yang C, Lou R Z. The newly emerged SARS-like coronavirus HCoV-EMC also has an "Achilles' heel": Current effective inhibitor targeting a 3C-like protease. *Protein Cell* 2013, 4(4): 248-250, doi: 10.1007/s13238-013-2841-3.

[12] Zhang L, Lin D, Sun X, Curth U, Drosten C, Sauerhering L, Becker S, Rox K, Hilgenfeld R. Crystal structure of SARS-CoV-2 main protease provides a basis for design of improved α-ketoamide inhibitors. *Science* 2020, 368, 409-412, doi: 10.1126/science.abb3405.

[13] Tang B, He F, Liu D, Fang M, Wu Z, Xu D. AI-aided design of novel targeted covalent inhibitors against SARS-CoV-2. *bioRxiv* 2020, doi: 10.1101/2020.03.03.972133.

[14] Fischer A, Sellner M, Neranjan S, Smiesko M, Lill M A. Potential inhibitors for novel Coronavirus protease identified by virtual screening of 606 million compounds. *Int. J. Mol. Sci.* 2020, 21, 3626, doi: 10.3390/ijms21103626.

[15] Ton A T, Gentile F, Hsing M, Ban F, Cherkasov A. Rapid Identification of Potential Inhibitors of SARS-CoV-2 Main Protease by Deep Docking of 1.3 Billion Compounds. *Mol. Inform*. 2020, 39(8), 2000028, doi: 10.1002/minf.202000028.

[16] Ou-Yang S S, Lu J Y, Kong X Q, Liang Z J, Luo C, Jiang H. Computational drug discovery. *Acta. Pharmacol. Sin.*, 2012, 33(9), 1131-1140, doi: 10.1038/aps.2012.109.

[17] Douguet D. Data Sets Representative of the Structures and Experimental Properties of FDA-Approved Drugs. *ACS Med. Chem. Lett.* 2018, 9(3), 204-209, doi: 10.1021/acsmedchemlett.7b00462.

[18] Berman H M, Westbrook J, Feng Z, Gilliland G, Bhat T N, Weissig H, Shindyalov I N, Bourne P E. The protein data bank. *Nucleic Acids Res*. 2000, 28(1), 235-342, doi: 10.1093/nar/28.1.235.

[19] Molecular Operating Environment, version 2014; Chemical Computing Group Inc: Montreal, Canada, 2010.

[20] Halgren T A. Merck molecular forcefield. *J. Comput. Chem*. 1996, 17, 490-641, doi: 10.1002/(SICI)1096-987X(199604)17:5/6<520::AID-JCC2>3.0.CO;2-W.

[21] Anand K, Palm G J, Mesters J R, Siddell S G, Ziebuhr J, Hilgenfeld R. Structure of coronavirus main proteinase reveals combination of a chymotrypsin fold with an extra alphahelical domain, *EMBO J.* 2002, 21(13), 3213-3224.

[22] Yoshino R, Yasuo N, Sekijima M. Identification of key interactions between SARS-CoV-2 main protease and inhibitor drug candidate. *Scientific Reports*, 2020, 10, 12493, doi: 10.1038/s41598-020-69337-9.

[23] Gentile D, Patamiia V, Scala A, Sciortino M T, Piperno A, Rescifina A. Putative Inhibitors of SARS-CoV-2 Main Protease from A Library of Marine Natural Products: A Virtual Screening and Molecular Modeling Study. *Mar. Drugs* 2020, 18, 225, doi: 10.3390/md18040225.

[24] Arun, K G, Sharanya C S, Abhithaj J, Francis D, Sadasivan C. Drug repurposing against SARS-CoV-2 using E-pharmacophore based virtual screening, molecular docking and molecular dynamics with main protease as the target. *J. Biomol. Struct. Dyn.* 2020, doi: 10.1080/07391102.2020.1779819.

[25] Ntie-Kang F, Nwodo N J, Ibezim A, Simoben C V, Karaman B, Ngwa V F, Sippl W, Adikwu U M, Mbaze L M. Molecular modeling of potential anticancer agents from African medicinal plants. *J. Chem. Inf. Model.* 2014, 54, 2433-2450, doi: 10.1021/ci5003697.

[26] DrugBank. Available online: https://www.drugbank.ca/drugs/ (Assessed on 25 August, 2020).

[27] Lipinski C A, Lombardo F, Dominy B W, Feeney P J. Experimental and computational approaches to estimate solubility and permeability in drug discovery and development settings. *Advanced Drug Delivery Reviews*. 2001, 46(1-3), 3-26, doi: 10.1016/S0169-409X(00)00129-0.

[28] Leeson P D, Springthorpe B. The influence of drug-like concepts on decision-making in medicinal chemistry. Nat. Rev. Drug Discov. 2007, 6(11): 881-890. doi: 10.1038/nrd2445.

How to cite this article:
Onah E, Ugwoke I.C, Eze U.J, Eze H.C, Musa S.K, Ndiana-Abasi S, Okoli O, Ekeh I.E. Edet A. A. Search for structural scaffolds against SARS-COV-2 M^{pro}: an *in silico* study. J. Fundam. Appl. Sci., 2021,*13(2), 740-769.*